Spin order and fluctuations in the $EuAl_4$ and $EuGa_4$ topological antiferromagnets: A μSR study

X. Y. Zhu [1,*] H. Zhang, [1,*] D. J. Gawryluk [2] Z. X. Zhen, [1] B. C. Yu, [1] S. L. Ju, [3] W. Xie, [4] D. M. Jiang, [1] W. J. Cheng, [1] Y. Xu, [1] M. Shi, [3] E. Pomjakushina, [2] Q. F. Zhan, [1] T. Shiroka [5,6,†] and T. Shang [1,‡]

[1] *Key Laboratory of Polar Materials and Devices (MOE), School of Physics and Electronic Science, East China Normal University, Shanghai 200241, China*

[2] *Laboratory for Multiscale Materials Experiments, Paul Scherrer Institut, Villigen CH-5232, Switzerland*

[3] *Swiss Light Source, Paul Scherrer Institut, Villigen CH-5232, Switzerland*

[4] *DESY, Notkestraβe 85, D-22607 Hamburg, Germany*

[5] *Laboratory for Muon-Spin Spectroscopy, Paul Scherrer Institut, Villigen PSI, Switzerland*

[6] *Laboratorium für Festkörperphysik, ETH Zürich, CH-8093 Zürich, Switzerland*

(Received 11 November 2021; revised 18 December 2021; accepted 6 January 2022; published 19 January 2022)

$EuAl_4$ and $EuGa_4$ are two candidate materials for studying the interplay between correlated-electron phenomena, topological spin textures, and topologically nontrivial bands. Both compounds crystallize in a centrosymmetric tetragonal $BaAl_4$-type structure (space group $I4/mmm$) and show antiferromagnetic (AFM) order below $T_N = 15.6$ and 16.4 K, respectively. Here, we report on systematic muon-spin rotation and relaxation (μSR) studies of the magnetic properties of $EuAl_4$ and $EuGa_4$ single crystals at a microscopic level. In both cases, transverse-field μSR measurements, spanning a wide temperature range (from 1.5 to 50 K), show clear bulk AFM transitions, with an almost 100% magnetic volume fraction. Zero-field μSR measurements, covering both the AFM and the paramagnetic (PM) states, reveal internal magnetic fields $B_{int}(0) = 0.33$ T and 0.89 T in $EuAl_4$ and $EuGa_4$, respectively. The transverse muon-spin relaxation rate λ_T, a measure of the internal field distribution at the muon-stopping site, shows a contrasting behavior. In $EuGa_4$, it decreases with lowering the temperature, reaching its minimum at zero temperature, $\lambda_T(0) = 0.71\ \mu s^{-1}$. In $EuAl_4$, it increases significantly below T_N, to reach 58 μs^{-1} at 1.5 K, most likely reflecting the complex magnetic structure and the competing interactions in the AFM state of $EuAl_4$. In both compounds, the temperature-dependent longitudinal muon-spin relaxation $\lambda_L(T)$, an indication of the rate of spin fluctuations, diverges near the onset of AFM order, followed by a significant drop at $T < T_N$. In the AFM state, spin fluctuations are much stronger in $EuAl_4$ than in $EuGa_4$, while being comparable in the PM state. The evidence of robust spin fluctuations against external magnetic fields provided by μSR may offer valuable insights into the origin of the topological Hall effect and the possible magnetic skyrmions in the $EuAl_4$ and $EuGa_4$ compounds.

DOI: 10.1103/PhysRevB.105.014423

I. INTRODUCTION

Topological materials are at the forefront of quantum matter and material science research due to their great potential for applications [1,2]. Recently, the discovery of nontrivial band topology and extremely large magnetoresistance in the $BaAl_4$ compound has stimulated considerable interest in this family of materials [3]. The tetragonal $BaAl_4$-type structure with a space group $I4/mmm$ (No. 139) represents the prototype for many binary- and ternary derivative compounds [4], as, e.g., heavy-fermion compounds and iron-based high-T_c superconductors.

Upon replacing Ba with Sr or Eu, or when replacing Al with Ga, all AE(Al,Ga)$_4$ (AE = Sr, Ba, and Eu) crystallize in the same tetragonal structure, while Ca(Al,Ga)$_4$ adopts a monoclinic crystal structure with a space group $C2/m$ (No. 12) [3,5]. Among these materials, the Eu-4f electrons bring new intriguing aspects to the topology. Both $EuAl_4$ and $EuGa_4$ are antiferromagnets below their critical temperatures $T_N = 15.6$, and 16.4 K, respectively, with the former also undergoing a CDW transition at $T_{CDW} \sim 140$ K [6–12]. Further, while $EuGa_4$ exhibits only one antiferromagnetic (AFM) transition, $EuAl_4$ undergoes four subsequent AFM transitions below T_N. More interestingly, by applying a magnetic field along the c axis, both $EuAl_4$ and $EuGa_4$ undergo a series of metamagnetic transitions in the AFM state [6,7,10]. Within a field range of ∼1–2.5 T ($EuAl_4$) or ∼4–7 T ($EuGa_4$), a clear hump-like anomaly was observed in the Hall resistivity, most likely a manifestation of the topological Hall effect (THE) [6,7]. Very recently, a THE has been observed also in Al-doped $EuGa_4$ [13], which exhibits comparable critical fields to $EuAl_4$ [6].

The topological Hall effect is considered to be the hallmark of spin textures with a finite scalar spin chirality. Such topological spin textures usually exhibit a nonzero Berry phase, here acting as an effective magnetic field, giving rise to the topological Hall resistivity [14]. THE is frequently observed in magnetic materials with noncoplanar spin textures, such as magnetic skyrmions [15–25]. Skyrmions are one of the most intriguing topologically nontrivial spin textures that can be

*These authors contributed equally to this work.
†Corresponding author: tshiroka@phys.ethz.ch
‡Corresponding author: tshang@phy.ecnu.edu.cn

easily manipulated [26], hence holding a promise for diverse applications, such as high-density spintronics [27,28]. THE has been observed mostly in magnetic compounds whose crystal structure lacks an inversion center, while centrosymmetric compounds that host magnetic skyrmions are rare [15–19,29,30]. Eu(Al,Ga)$_4$ represent such rare cases, where to look for the possible existence of magnetic skyrmions [6,7,13]. According to neutron diffraction studies, in the AFM state, the magnetic q vector of $EuAl_4$ changes from $\boldsymbol{q}_1 = (0.085, 0.085, 0)$ at $T_N = 13.5$ K to $\boldsymbol{q}_2 = (0.170, 0, 0)$ at 11.5 K and slightly to $\boldsymbol{q}_3 = (0.194, 0, 0)$ at 4.3 K [31]. Unlike the complex incommensurate transitions observed in $EuAl_4$, the AFM structure of $EuGa_4$ is described by a simple $\boldsymbol{q} = (0, 0, 0)$ magnetic vector, with the Eu moments lying in the basal ab plane [32]. Noncollinear spins with incommensurate propagation vectors have been reported also in the isostructural $EuGa_2Al_2$ [13].

As an extremely sensitive magnetic probe at a microscopic level, the muon-spin rotation and relaxation (μSR) technique lends itself naturally to studying the temperature evolution of the magnetic properties of $EuAl_4$ and $EuGa_4$ single crystals. As shown in detail below, we report: (i) the intrinsic fields at the muon implantation sites in $EuAl_4$ and $EuGa_4$ across the respective phase diagrams in the absence of external magnetic fields; (ii) the magnetic volume fraction in the AFM state; (iii) evidence of strong spin fluctuations.

II. EXPERIMENTAL DETAILS

Single crystals of $EuAl_4$ and $EuGa_4$ were grown by a molten Al- and Ga-flux method, respectively, the details of growth being reported elsewhere [6,7]. The crystal orientation was checked by x-ray diffraction (XRD) measurements using a Bruker D8 diffractometer with Cu K_α radiation. The magnetic susceptibility measurements were performed on a Quantum Design magnetic properties measurement system (MPMS) with the applied magnetic field along the c axis.

μSR experiments were carried out at the general-purpose surface-muon (GPS) instrument at the πM3 beam line of the Swiss muon source (SμS) at Paul Scherrer Institut (PSI) in Villigen, Switzerland. In this study, we performed three kinds of experiments: weak transverse-field (wTF)-μSR, zero-field (ZF)-, and longitudinal-field (LF)-μSR measurements. As to the former, we could determine the temperature evolution of the magnetic volume fraction. As to the latter two, we aimed at studying the temperature evolution of the magnetically ordered phase and the dynamics of spin fluctuations.

The aligned $EuAl_4$ and $EuGa_4$ crystals were positioned on a thin aluminum tape, with their c axes parallel to the muon-momentum direction, i.e., $\boldsymbol{p}_\mu \parallel c$ [see inset in Fig. 1(a)]. For the wTF-μSR measurements, the applied magnetic field B_{appl} was perpendicular to the muon-spin direction (i.e., $B_{\text{appl}} \perp \boldsymbol{S}_\mu$), while it was parallel for the LF-μSR measurements (i.e., $B_{\text{appl}} \parallel \boldsymbol{S}_\mu$). In both wTF- and LF-$\mu$SR cases, the crystals were cooled in an applied magnetic field down to the base temperature (i.e., 1.5 K). For the ZF-μSR measurements, to exclude the possibility of stray magnetic fields, the magnets were degaussed before the measurements. All the μSR spectra were collected upon heating and were analyzed by means of the `musrfit` software package [33].

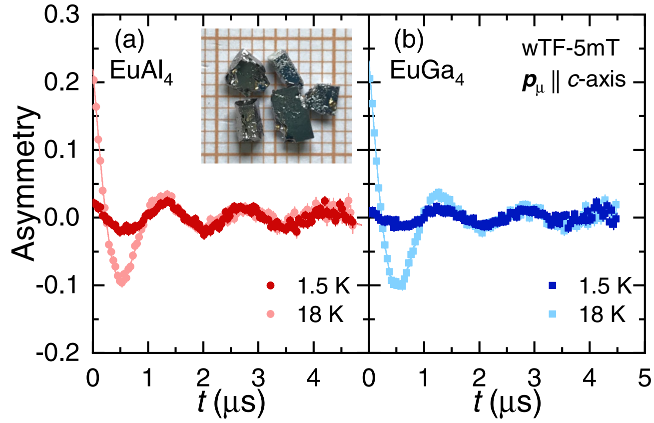

FIG. 1. Time-domain wTF-μSR spectra of (a) $EuAl_4$ and (b) $EuGa_4$ single crystals, collected in the AFM (1.5 K) and PM (18 K) states in a weak transverse field of 5 mT. The solid lines represent fits to Eq. (1). The inset in (a) depicts the $EuAl_4$ crystals, aligned with their c axis parallel to the muon momentum direction, i.e., $\boldsymbol{p}_\mu \parallel c$.

III. RESULTS AND DISCUSSION

A. wTF-μSR

The magnetic transition temperatures T_N and the evolution with temperature of the magnetic volume fraction in $EuAl_4$ and $EuGa_4$ single crystals were established by means of wTF-μSR measurements. A weak transverse field of 5 mT was applied perpendicular to the initial muon-spin direction in the PM state, where it leads to oscillations, as shown in Fig. 1. In the long-range ordered AFM state (i.e., 1.5 K), the applied 5-mT field is much smaller than the internal fields. As a consequence, upon entering the AFM state, muon spins precess with frequencies that reflect the internal fields at the muon-stopping sites rather than the weak applied field. Normally, the magnetic order leads to a very fast muon-spin depolarization in the first tenths of μs (see also the ZF-μSR spectra in the insets of Fig. 3). Therefore, the wTF-μSR spectra can be described by the function:

$$A_{\text{wTF}}(t) = A_{\text{NM}} \cos(\gamma_\mu B_{\text{int}} t + \phi) \cdot e^{-\lambda t}, \tag{1}$$

where A_{NM} is the initial muon-spin asymmetry (i.e., the amplitude of the oscillation) for muons implanted in the nonmagnetic (NM) or PM fraction of $EuAl_4$ and $EuGa_4$ single crystals; $\gamma_\mu B_{\text{int}}$ is the muon-spin precession frequency, with $\gamma_\mu = 2\pi \times 135.5$ MHz/T the muon gyromagnetic ratio and B_{int} the local field sensed by muons (here almost identical to the applied magnetic field, i.e., $B_{\text{int}} \sim 5$ mT); ϕ is the initial phase, and λ is the muon-spin relaxation rate. Note that, in the AFM state, the very fast μSR relaxation was excluded and only the residual slow-relaxing asymmetry was analyzed (see the 1.5-K dataset in Fig. 1).

Figure 2 summarizes the resulting wTF-μSR asymmetry values A_{NM} as a function of temperature. In the PM state, all the implanted muons precess at the same frequency $\gamma_\mu B_{\text{int}}$. As the temperature approaches T_N, only the muons implanted in the remaining PM/NM phase precess at the frequency $\gamma_\mu B_{\text{int}}$, here reflected in the progressive reduction of the asymmetry. The PM (or NM) sample fraction is determined from

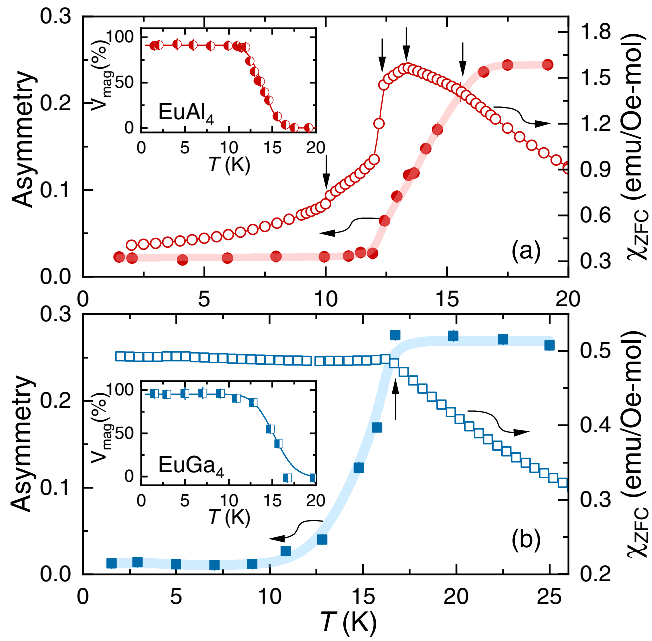

FIG. 2. Temperature dependence of the $A_{\rm NM}$ asymmetry (left axis) of wTF-μSR spectra for (a) $EuAl_4$ and (b) $EuGa_4$ single crystals. We report also the magnetic susceptibilities $\chi_{\rm ZFC}$ (right axes), measured in a field of $\mu_0 H = 0.1$ T after zero-field cooling (ZFC). In both cases, the insets show the magnetic volume fraction vs temperature. Here, lines are fits to a phenomenological function [see Eq. (2)]. The vertical arrows mark the AFM transitions. The magnetic susceptibility data were taken from Refs. [6,7].

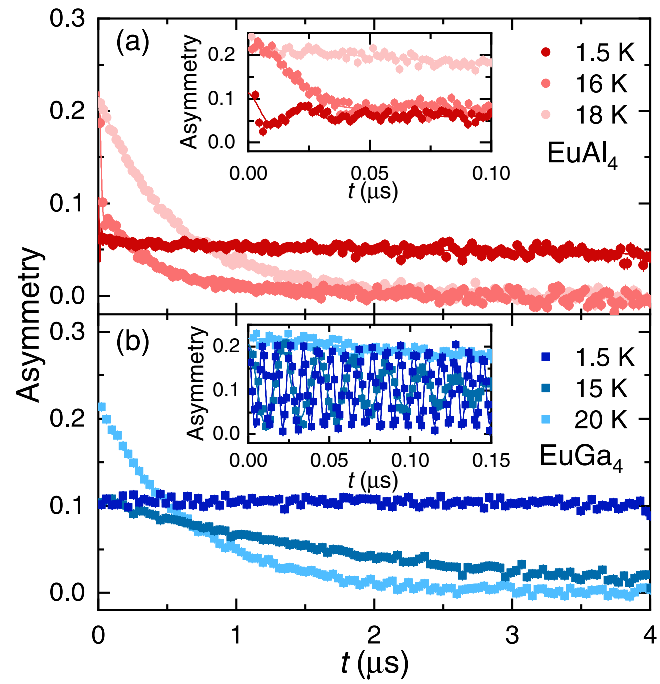

FIG. 3. Representative ZF-μSR spectra collected in a transverse muon-spin configuration ($\boldsymbol{p}_\mu \perp \boldsymbol{S}_\mu$) at temperatures covering both the PM and AFM states for (a) $EuAl_4$ and (b) $EuGa_4$, respectively. Insets highlight the short-time spectra, illustrating the coherent oscillations caused by the long-range AFM order. Solid lines through the data are fits to Eq. (3) (see text for details).

the oscillation amplitude. In both $EuAl_4$ and $EuGa_4$, $A_{\rm NM}$ starts to decrease near the onset of AFM order, where also the magnetic susceptibilities show clear transitions. Although $EuAl_4$ undergoes four successive AFM transitions [indicated by vertical arrows in Fig. 2(a)], $A_{\rm NM}(T)$ does not capture them individually, as it is sensitive only to the global PM (or NM) volume fraction. The temperature evolution of the magnetic volume fraction can be derived from $V_{\rm mag}(T) = 1 - A_{\rm NM}(T)/A_{\rm NM}(T > T_{\rm N})$. The $V_{\rm mag}(T)$ values are summarized in the insets of Fig. 2(a) and 2(b) for $EuAl_4$ and $EuGa_4$, respectively. To determine the magnetic volume fraction $V_{\rm mag}$, the average magnetic transition temperature $T_{\rm N}$, and the transition width ΔT, $V_{\rm mag}(T)$ data were fitted using the phenomenological function:

$$V_{\rm mag}(T) = V_{\rm mag}(0)\,\frac{1}{2}\left[1 - \mathrm{erf}\left(\frac{T - T_{\rm N}}{\sqrt{2}\Delta T}\right)\right], \quad (2)$$

where $\mathrm{erf}(T)$ is the error function. As shown by solid lines in the insets of Fig. 2, for $EuAl_4$, we obtain $T_{\rm N} = 13.9(2)$ K, $\Delta T = 1.4(2)$ K, and $V_{\rm mag}(0) = 91(2)\%$, while for $EuGa_4$, $T_{\rm N} = 15.2(3)$ K, $\Delta T = 1.8(2)$ K, and $V_{\rm mag}(0) = 95(2)\%$. Both samples show sharp transitions and can be considered as fully magnetically ordered at low temperatures, indicative a high sample quality. Note also that the transition temperatures, as determined from $V_{\rm mag}(T)$, have their onset at $\sim$16.5 K and $\sim$16.7 K for $EuAl_4$ and $EuGa_4$, both in very good agreement with the magnetometry data.

B. ZF- and LF-μSR

To investigate the local magnetic order of $EuAl_4$ and $EuGa_4$ single crystals, ZF-μSR spectra were collected at different temperatures, covering both the PM and AFM states. The time evolution of ZF-μSR asymmetry, $A_{\rm ZF}(t)$, encodes the intrinsic magnetic fields and their distribution at the muon-stopping site. If the electronic magnetic moments fluctuate very fast (typically above 10^{12} Hz in the PM state), they do not influence the muon-spin polarization. Randomly oriented slow fluctuating or static moments (below 10^4 Hz, such as nuclear spins, or electronic moments in spin glasses), give rise to incoherent precessions and a slow depolarization. Conversely, in case of ordered static moments, a fast depolarization and superimposed oscillations, reflecting the coherent precession of the muon spins, are observed [34]. This is clearly demonstrated in Fig. 3, where the time evolution of selected ZF-μSR spectra for $EuAl_4$ and $EuGa_4$ are presented.

In the PM state ($T > T_{\rm N}$), the μSR spectra still exhibit a relatively fast muon-spin depolarization ($\sim$2 μs^{-1}), implying the existence of strong spin fluctuations, here further confirmed by LF-μSR measurements (see below). In the absence of spin fluctuations, the muon-spin depolarization is usually due to the nuclear dipole fields [34], with a typical value of less than 0.1 μs^{-1} in $EuAl_4$ and $EuGa_4$ [35]. The μSR spectra in the AFM state ($T \leqslant T_{\rm N}$) are characterized by highly damped oscillations, typical of long-range magnetic order (see insets in Fig. 3), superimposed on a slowly decaying relaxation, observable only at long times. To track these changes across the whole temperature range, the ZF-μSR spectra of

$EuAl_4$ and $EuGa_4$ were analyzed using the following model:

$$A_{ZF}(t) = A_1 \cdot \left[\alpha \cos(\gamma_\mu B_{int} t + \phi) \cdot e^{-\lambda_T t} + (1-\alpha) \cdot e^{-\lambda_L t}\right] + A_2 \cdot e^{-\lambda_{tail} t}. \quad (3)$$

Here, α and $1-\alpha$ are the oscillating (i.e., transverse) and nonoscillating (i.e., longitudinal) fractions of the μSR signal, respectively, whose initial total asymmetry is equal to A_1. λ_T and λ_L represent the transverse and longitudinal relaxation rates, while A_1 and A_2 represent the asymmetries of the two nonequivalent muon-stopping sites. In $EuAl_4$, muons stopping at the second site do not undergo any precession but show only a slow relaxation, here described by λ_{tail}. In $EuGa_4$, a single muon-stopping site is sufficient to describe the ZF-μSR spectra. Finally, B_{int}, ϕ, and γ_μ are the same as in Eq. (1). Similar expressions have been used to analyze the μSR data in other Eu-based magnetic materials, most notably, in the Eu122 iron pnictides [36,37].

In polycrystalline materials with a long-range magnetic order, one expects $\alpha = 2/3$, since statistically one third of the muon spins are aligned parallel to the local field direction (i.e., $\boldsymbol{S}_\mu \parallel B_{int}$) and, hence, do not precess. In $EuAl_4$ and $EuGa_4$ single crystals, we find α to be 0.87 and 0.46, respectively. Since the ZF-μSR spectra were collected in a rotated muon-spin configuration (i.e., $\boldsymbol{S}_\mu \perp \boldsymbol{p}_\mu$), and the c axis is parallel to the muon momentum (i.e., $c \parallel \boldsymbol{p}_\mu$), the internal magnetic fields at the muon-stopping sites should be mostly aligned along the [001] direction in $EuAl_4$ but along the [111] direction in $EuGa_4$.

The derived fit parameters for both cases are summarized in Figs. 4 and 5. As can be clearly seen in the top panels, $EuAl_4$ and $EuGa_4$ show rather different $B_{int}(T)$ behaviors. In $EuAl_4$, the $B_{int}(T)$ undergoes a sudden drop at $\sim$13 K, which corresponds to the second AFM transition in the magnetic susceptibility [see Fig. 2(a)]. Conversely, in $EuGa_4$, $B_{int}(T)$ resembles the typical mean-field type curve below T_N. Since B_{int} is directly proportional to the magnetic moment, the evolution of B_{int} reflects that of the magnetic structure. According to neutron scattering studies, in $EuAl_4$, the magnetic q vector changes from $\boldsymbol{q}_1 = (0.085, 0.085, 0)$ at $T_N = 13.5$ K to $\boldsymbol{q}_2 = (0.170, 0, 0)$ at 11.5 K and slightly to $\boldsymbol{q}_3 = (0.194, 0, 0)$ at 4.3 K [31]. Therefore, we identify the drop of B_{int} at 13 K with the critical temperature where the magnetic structure changes from q_1 to q_2. At the same time, the modification of magnetic structure from q_2 to q_3 is too tiny to have a measurable effect on B_{int}. By contrast, the AFM structure of $EuGa_4$ is rather simple [its magnetic vector being $\boldsymbol{q} = (0, 0, 0)$] and it persists down to 2 K [32]. As a consequence, in $EuGa_4$, B_{int} decreases monotonically as the temperature increases. In both compounds, $B_{int}(T)$ can be modeled by the phenomenological equation:

$$B_{int}(T) = B_{int}(0) \cdot \left[1 - \left(\frac{T}{T_N}\right)^\gamma\right]^\delta. \quad (4)$$

Here, $B_{int}(0)$ is the internal magnetic field at zero temperature, while γ and δ are two empirical parameters. As indicated by the solid lines in Figs. 4(a) and 5(a), the above model describes the data reasonably well, yielding the parameters listed in Table I. In $EuAl_4$, the first AFM phase (AFM1) is characterized by $B_{int}(0) = 0.57(5)$ T. The change in magnetic

TABLE I. Summary of the $EuAl_4$ and $EuGa_4$ single-crystal parameters obtained by means of magnetization and μSR measurements.

	T_N^χ(K)	$T_N^{\mu SR}$(K)[a]	$T_N^{\mu SR}$(K)[b]	B_{int}(T)	γ	δ
$EuAl_4^{AFM1}$	15.6(2)	13.9(1)	16.0(2)	0.57(5)	2.50(5)	0.50(5)
$EuAl_4^{AFM2}$	12.3(3)		13.7(4)	0.33(2)	0.92(5)	0.17(3)
$EuGa_4$	16.5(2)	15.2(3)	16.5(4)	0.89(2)	1.50(5)	0.50(5)

[a]Determined from the asymmetry of wTF-μSR spectra.
[b]Determined from fits of ZF-μSR spectra.

structure lowers $B_{int}(0)$ down to 0.33(2) T in the second AFM phase (AFM2). In $EuGa_4$, $B_{int}(T)$ follows the typical mean-field type curve, yielding $B_{int}(0) = 0.89(2)$ T. Considering the presence of the same magnetic Eu^{2+} ions in both cases and the similar lattice parameters, the significantly different $B_{int}(0)$ values are most likely attributed to the different muon-stopping sites or to different magnetic structures in $EuAl_4$ and $EuGa_4$, the latter having been proved by neutron scattering studies. Indeed, at base temperature, $EuAl_4$ exhibits a complex incommensurate magnetic structure, while this is commensurate in $EuGa_4$ [31,32].

The temperature dependence of the transverse and longitudinal μSR relaxation rates $\lambda_T(T)$ and $\lambda_L(T)$ are summarized in Figs. 4(b) and 4(c) for $EuAl_4$ and in Figs. 5(b) and 5(c) for $EuGa_4$, respectively. The transverse relaxation rate λ_T is a measure of the width of static magnetic field distribution at the muon-stopping site and is also affected by dynamical effects, as e.g., spin fluctuations. The longitudinal relaxation rate λ_L is determined solely by spin fluctuations. In $EuAl_4$ and $EuGa_4$, $\lambda_T(T)$ exhibits clearly opposite behaviors. In $EuAl_4$ [see Fig. 4(b)], λ_T is zero in the PM state, and becomes increasingly prominent as the temperature decreases below T_N, reflecting a more disordered field distribution well inside the AFM state. Such a large λ_T at temperatures far below T_N is unusual for an antiferromagnet and implies an increasingly inhomogeneous distribution of local fields in the AFM state of $EuAl_4$. Thus, at 1.5 K, $\lambda_T \sim 58(10)\ \mu s^{-1}$, which implies a half width at half maximum (HWHM) of field distribution $\Delta = 68(12)$ mT (here, $\Delta = \lambda_T/\gamma_\mu$). Such enhanced local-field distribution might be related to the complex spatial arrangement of the Eu magnetic moments in $EuAl_4$, where the magnetic propagation vector is incommensurate with the crystal lattice [31]. By contrast, in $EuGa_4$, $\lambda_T(T)$ follows the typical behavior of materials with a long-range (anti)ferromagnetic order [36], i.e., diverging at T_N and continuously decreasing at $T < T_N$. Such $\lambda_T(T)$ suggests a very homogeneous distribution of local fields, consistent with the commensurate magnetic propagation vector in $EuGa_4$ [32]. At $T = 1.5$ K, in $EuGa_4$, λ_T is found to be $\sim$0.72 μs^{-1}, a value which is almost three orders of magnitude smaller than that of $EuAl_4$. This is also reflected in the ZF-μSR spectra shown in the insets of Fig. 3, where the damping of the muon-spin precession is much weaker in $EuGa_4$ than in $EuAl_4$.

The longitudinal μSR relaxation rates λ_L shown in Figs. 4(c) and 5(c) are much smaller than the transverse relaxation rates λ_T. At 1.5 K, $\lambda_L/\lambda_T \sim 0.15$ and 0.02 for $EuAl_4$ and $EuGa_4$, respectively. In contrast to $\lambda_T(T)$ [see Figs. 4(b) and 5(b)], $EuAl_4$ and $EuGa_4$ exhibit a similar

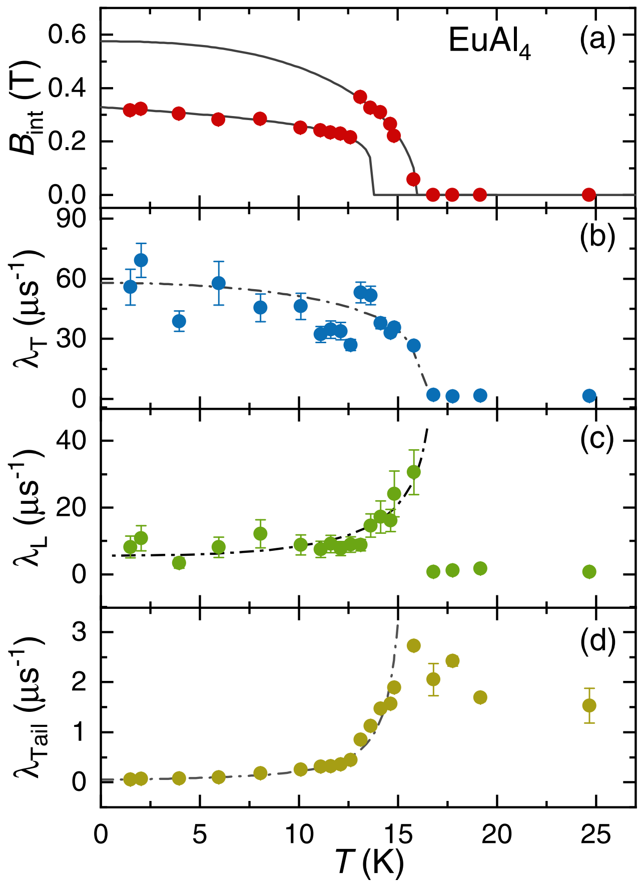

FIG. 4. Temperature dependence of (a) internal field $B_{\rm int}(T)$, (b) transverse muon-spin relaxation rate (known also as damping rate) $\lambda_{\rm T}(T)$, and (c) longitudinal muon-spin relaxation rate $\lambda_{\rm L}(T)$ for $EuAl_4$, as derived from ZF-μSR analysis. The muon-spin relaxation rate of the tail of the ZF-μSR spectra, $\lambda_{\rm tail}$, is shown in panel (d). Solid lines are fits to the equations described in the text; dash-dotted lines are guides to the eyes.

temperature-dependent $\lambda_{\rm L}(T)$, typical of materials with long-range magnetic order. In both cases, $\lambda_{\rm L}(T)$ diverges near $T_{\rm N}$, followed by a significant drop at $T < T_{\rm N}$, indicating that spin fluctuations are the strongest close to the onset of the AFM order. At 1.5 K, $\lambda_{\rm L}$ is 8.2 and 0.01 μs^{-1} in $EuAl_4$ and $EuGa_4$, respectively. In $EuAl_4$, at temperatures well inside the AFM state, $\lambda_{\rm L}$ is hundreds of times larger than in $EuGa_4$, thus suggesting much stronger spin fluctuations in the AFM state of $EuAl_4$ than in $EuGa_4$. Conversely, in the PM state, both $EuAl_4$ and $EuGa_4$ exhibit similar $\lambda_{\rm L}$ values. Note that, in $EuAl_4$, as shown in Fig. 4(d), muons implanted in the second site experience only the spin fluctuations. Consequently, $\lambda_{\rm tail}(T)$ in $EuAl_4$ shows similar features to $\lambda_{\rm L}(T)$, i.e., it exhibits a maximum near the onset of the AFM order and it, too, decreases as the temperature is lowered. Future calculations of the muon-stopping sites might be helpful to better appreciate the differences between $EuAl_4$ and $EuGa_4$. In the fast-fluctuation limit (typical of magnetically ordered materials), the zero-field longitudinal muon-spin relaxation rate is described by:

$$\lambda_{\rm L} = \frac{2\gamma_\mu^2 \Delta^2}{\nu}, \tag{5}$$

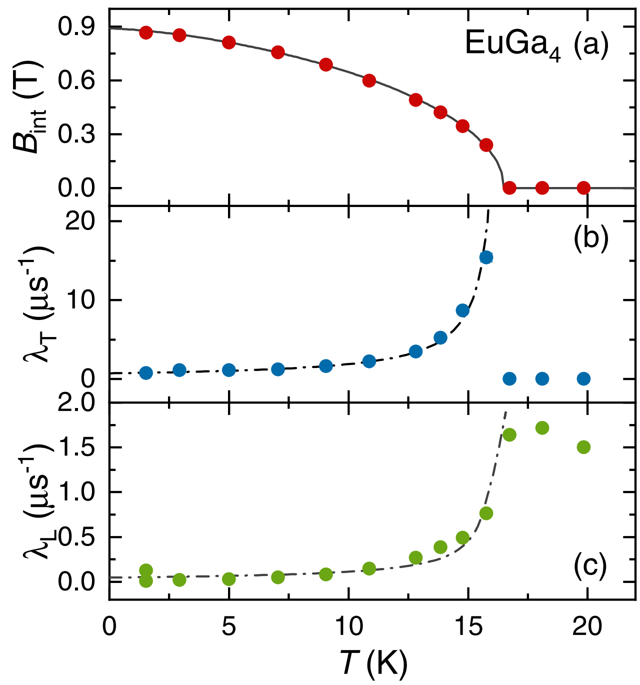

FIG. 5. Temperature dependence of (a) internal field $B_{\rm int}(T)$, (b) transverse muon-spin relaxation rate (i.e., damping rate) $\lambda_{\rm T}(T)$, and (c) longitudinal muon-spin relaxation rate $\lambda_{\rm L}(T)$ for $EuGa_4$, as derived from ZF-μSR analysis. Solid lines are fits to the equations described in the text; dash-dotted lines are guides to the eyes.

where Δ is the amplitude of field fluctuations, while ν is their correlation frequency (i.e., $1/\nu = \tau$, is the spin-correlation time) [34]. The estimated spin-correlation times are $\tau = 1.3$ and 8.2 ns for $EuAl_4$ and $EuGa_4$, respectively.

The vigorous spin fluctuations in these compounds are further supported by LF-μSR measurements. As shown in Fig. 6, the μSR spectrum in a 0.7-T longitudinal field is almost identical to that collected in a zero-field condition, suggesting that muon spins cannot be decoupled, hence, that spin fluctuations survive even in a field of 0.7 T in both $EuAl_4$ and $EuGa_4$. Note that, such spin fluctuations are robust against external magnetic fields, both in the AFM (e.g., 1.5 K) and in the PM states (i.e., 50 K) far above $T_{\rm N}$ (see details in Fig. 7 in the Appendix). Similar μSR results have been reported in other Eu-based materials, e.g., $EuCd_2As_2$, where the strong spin fluctuations cause the breaking of time-reversal symmetry and lead to the formation of magnetic Weyl fermions [38].

C. Discussion

First we discuss why the successive magnetic transitions of $EuAl_4$ remain undetected by μSR measurements, an absence which might be due to different reasons. Firstly, the asymmetries obtained from wTF-μSR (see Figs. 1 and 2) reflect the internal fields sensed by the implanted muons. However, when the applied transverse field is much smaller than the internal fields, the wTF signal is mostly determined by the muons implanted in the residual NM (or PM) fraction of a magnetically ordered sample. This is reflected in a significant drop of

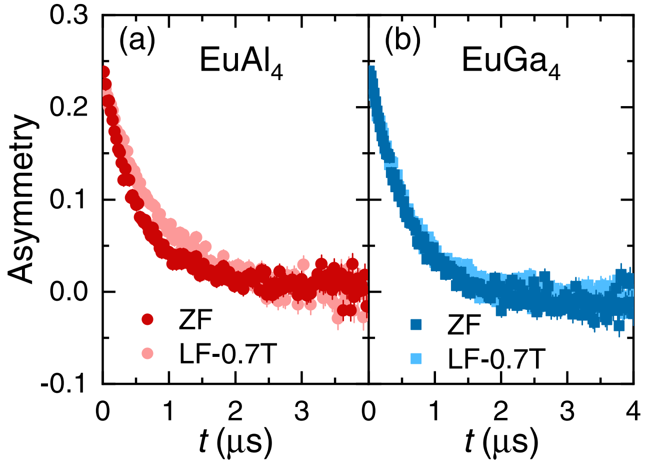

FIG. 6. LF-μSR time-domain spectra collected at 18 K (i.e., slightly above T_N) in an applied magnetic field of 0 and 0.7 T in (a) $EuAl_4$ and (b) $EuGa_4$. Both spectra were collected in a longitudinal muon-spin configuration, i.e., $\boldsymbol{p}_\mu \parallel \boldsymbol{S}_\mu$. The applied magnetic field is parallel to the muon-spin direction. In either case, no appreciable decoupling of muon spins with field can be identified.

the temperature-dependent asymmetry $A(T)$. In $EuAl_4$, below the onset of AFM order, the internal fields are hundreds of times larger than the applied wTF. Although changes in the magnetic structure, detected as successive transitions in the $EuAl_4$ magnetometry data, decrease the internal field from ~0.4 T to 0.33 T, this still remains much larger than wTF. Therefore, the successive magnetic transitions of $EuAl_4$ are not easily detectable via wTF-μSR measurements. Secondly, a slight change/rearrangement of the magnetic structure does not have a large impact on the internal field. According to neutron scattering studies, in $EuAl_4$, the magnetic q vector changes from $\boldsymbol{q}_1 = (0.085, 0.085, 0)$ at $T_N = 13.5$ K to $\boldsymbol{q}_2 = (0.170, 0, 0)$ at 11.5 K and slightly to $\boldsymbol{q}_3 = (0.194, 0, 0)$ at 4.3 K [31]. Therefore, we identify the drop of B_{int} at 13 K with the critical temperature where the magnetic structure changes from q_1 to q_2. At the same time, the modification of magnetic structure from q_2 to q_3 with the magnetic moments pointing at the same direction is too tiny to have a measurable effect on B_{int}. Thirdly, changes in magnetic structure have little effect on the longitudinal relaxation rates λ_L, which reflect solely the spin fluctuations in $EuAl_4$. In general, spin fluctuations decrease significantly as the temperature moves away from T_N, but they diverge near the onset of the magnetic transition. Hence, in the magnetically ordered state, changes in λ_L caused by slight modifications of the magnetic structure are negligible compared to the temperature driven effects.

Since most of the skyrmion phases appear in a field range not easily accessible by standard μSR instruments, up to now, only a handful of results have been reported where LF-μSR could be used to study skyrmion-hosting compounds. These include $GaV_4(S,Se)_8$ [39], Cu_2OSeO_3 [40], and the Co-Zn-Mn alloy [40,41], whose skyrmion phases are stabilized by a relatively small field (< 0.1 T). However, for many newly discovered skyrmion systems, i.e., $GdRu_2Si_2$ and $Gd_3Ru_4Al_{12}$ (as well as for $EuAl_4$ and $EuGa_4$ studied here) [6,7,29,30], the critical field required for stabilizing the skyrmion phase is above 1 T. In their AFM state, $EuAl_4$ and $EuGa_4$ exhibit comparable spin fluctuations to other well-studied skyrmion compounds. For instance, the muon-spin relaxation rates extracted from LF-μSR measurements in the skyrmion phases of Cu_2OSeO_3 and $GaV_4(S,Se)_8$ are ~0.2–0.8 μs^{-1}, similar to those of $Eu(Al,Ga)_4$ (see Figs. 4 and 5). All these skyrmion compounds exhibit similar temperature-dependent muon-spin relaxation rates $\lambda_L(T)$, with an enhanced and broadened peak in $\lambda_L(T)$ at temperatures just below the critical temperature. Muon-spin relaxation rates also increase when entering the skyrmion phase by applying longitudinal magnetic fields, thus providing another method for identifying the presence of magnetic skyrmions. In the $EuAl_4$ and $EuGa_4$ case, where there is no skyrmion phase in zero field, the relaxation rates diverge at T_N, followed by a significant drop at $T < T_N$ due to the slowing down of spin fluctuations, a typical feature of magnetically ordered materials. A similar behavior is observed in $Co_{10}Zn_{10}$ [40], a parent compound of the Co-Mn-Zn alloys, which lacks any skyrmion phases. According to Hall-resistivity measurements, the skyrmion phase may exist in a field range ~1–2.5 T in $EuAl_4$ and ~4–7 T in $EuGa_4$ [6,7]. Aimed at investigating the intrinsic magnetic properties of both compounds, most of the current μSR studies are performed in zero-field conditions. To compare the muon-spin relaxation rates of $EuAl_4$ and $EuGa_4$ with those of other skyrmion compounds, and to check if there are any skyrmion phases, further temperature-dependent μSR measurements under high magnetic fields are required.

The observation of a topological Hall effect in the magnetic state is usually attributed to noncoplanar spin textures, such as magnetic skyrmions, characterized by a finite scalar spin chirality in real space. These magnetic skyrmions are stabilized by the Dzyaloshinskii-Moriya interaction, often observed in noncentrosymmetric materials [42–48]. Conversely, magnetic materials with a centrosymmetric crystal structure that still host magnetic skyrmions are rare. To date, only a few systems have been reported, including some gadolinium intermetallic compound [19,29,30], Fe_3Sn_2 [49], and possibly, also $EuCd_2As_2$ [50]. In centrosymmetric systems, skyrmions can be stabilized, for instance, by magnetic frustration (e.g., in $Gd_3Ru_4Al_{12}$, Gd_2PdSi_3, and Fe_3Sn_2), or by the competition between the magnetic interactions and magnetic anisotropies (e.g., in $GdRu_2Si_2$) [19,29,30,49,51]. According to magnetization and nuclear magnetic resonance studies, $EuAl_4$ and $EuGa_4$ exhibit a moderate magnetic anisotropy [6,7,52]. Since both $EuAl_4$ and $EuGa_4$ adopt the same crystal structure of $GdRu_2Si_2$, skyrmions might be stabilized by the same mechanism. In addition, a four-spin interaction, mediated by itinerant electrons, has also been proposed as an important ingredient for the formation of skyrmions in centrosymmetric materials [51,53,54]. Very recently, the chiral magnet $Co_7Zn_7Mn_6$ was found to host a skyrmion phase far below the magnetic ordering temperature, where spin fluctuations are believed to be the key for stabilizing the magnetic skyrmions [41]. Our μSR results reveal that both $EuAl_4$ and $EuGa_4$ exhibit robust spin fluctuations against external magnetic fields, which analogously might be crucial for understanding the origin of topological Hall effect and of possible skyrmions in both materials.

IV. CONCLUSION

In summary, we investigated the temperature evolution of the local magnetic properties of $EuAl_4$ and $EuGa_4$ by means of μSR spectroscopy. wTF-μSR measurements confirm that $EuAl_4$ and $EuGa_4$ undergo an AFM transition at $T_N \sim 16$ and 16.5 K, which are consistent with the magnetization data. The magnetic volume fractions, as determined from wTF-μSR asymmetry, are 91% and 95% for $EuAl_4$ and $EuGa_4$, respectively, implying a good sample quality in both cases. By using ZF-μSR measurements, we could follow the temperature evolution of the local magnetic fields and of spin fluctuations. The estimated internal fields at zero temperature are 0.33 and 0.89 T for $EuAl_4$ and $EuGa_4$, respectively. $EuAl_4$ exhibits a more disordered internal field distribution than $EuGa_4$, reflected in a large transverse muon-spin relaxation rate λ_T far below T_N, most likely related to its complex magnetic structure. The vigorous spin fluctuations revealed by both ZF-μSR and LF-μSR might be crucial for understanding the origin of topological Hall effect and of possible skyrmions in $EuAl_4$ and $EuGa_4$. In future, it might be interesting to investigate the magnetic properties of $EuAl_4$ and $EuGa_4$ using the μSR technique under high magnetic fields, where the topological Hall effect appears.

ACKNOWLEDGMENTS

T.S. acknowledges support from the Natural Science Foundation of Shanghai (Grants No. 21ZR1420500 and No. 21JC1402300) and the Schweizerische Nationalfonds zur Förderung der Wissenschaftlichen Forschung (SNF) (Grants No. 200021_188706 and No. 206021_139082). Y.X. acknowledges support from the Shanghai Pujiang Program (Grant No. 21PJ1403100). This work was also financially supported by the National Natural Science Foundation of China (NSFC) (Grants No. 12174103 and No. 11874150) and the Sino-Swiss Science and Technology Cooperation (Grant No. IZLCZ2-170075). We thank G. Lamura for the assistance during some phases of the LF-μSR experiments.

APPENDIX: LONGITUDINAL-FIELD μSR in $EuAl_4$

In Fig. 7 we present the ZF- and LF-μSR spectra of $EuAl_4$, collected at temperatures well inside the AFM state (1.5 K) and far above T_N, in the PM state (i.e., 50 K). In the AFM state [see Fig. 7(a)], the fast drop of the μSR asymmetry reflects a very fast muon-spin depolarization in the first tenths of μs [see also ZF-μSR data in Fig. 3(a)]. A 0.78-T longitudinal magnetic field has negligible effects on the long-time μSR spectra. Indeed, both the ZF- and LF-μSR spectra are almost identical, implying that the spin fluctuations persist deep inside the AFM state of $EuAl_4$. Surprisingly, similar features are observed also in the PM state, as clearly demonstrated in Fig. 7(b) [see also Fig. 6]. Since the data suggest that muon spins cannot be decoupled neither in the AFM nor in the PM state, this implies that, in this type of materials, *spin fluctuations exist over a wide temperature range*, well above the AFM transition. We recall that, according to previous μSR studies on $EuCd_2As_2$, spin fluctuations are strongly enhanced below 100 K, thus causing the breaking of time-reversal symmetry and leading to the formation of magnetic Weyl fermions [38]. Further measurements at higher temperatures, including both ZF- and LF-μSR, are highly desirable to check if a similar phenomenology occurs also in the $BaAl_4$-type family of materials.

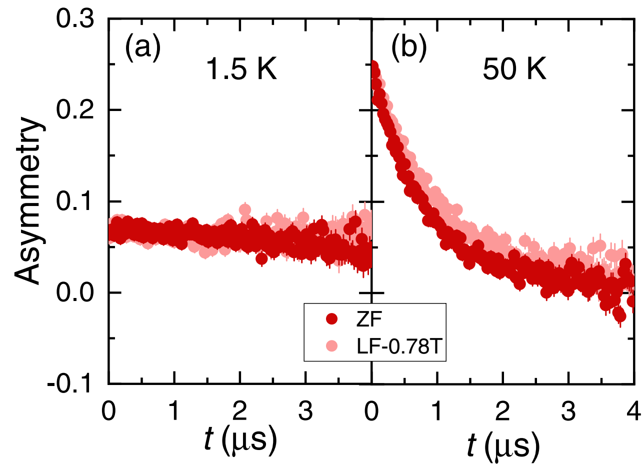

FIG. 7. LF-μSR time-domain spectra collected at 1.5 K (a) (far below T_N) and 50 K (b) (far above T_N) in an applied magnetic field of 0 and 0.78 T in $EuAl_4$. Both spectra were collected in a longitudinal muon-spin configuration, i.e., $\boldsymbol{p}_\mu \parallel \boldsymbol{S}_\mu$. The applied magnetic field is parallel to the muon-spin direction.

[1] N. P. Armitage, E. J. Mele, and A. Vishwanath, Weyl and Dirac semimetals in three-dimensional solids, Rev. Mod. Phys. **90**, 015001 (2018).

[2] B. Q. Lv, T. Qian, and H. Ding, Experimental perspective on three-dimensional topological semimetals, Rev. Mod. Phys. **93**, 025002 (2021).

[3] K. Wang, R. Mori, Z. Wang, L. Wang, J. H. S. Ma, D. W. Latzke, D. E. Graf, J. D. Denlinger, D. Campbell, B. A. Bernevig, A. Lanzara, and J. Paglione, Crystalline symmetry-protected non-trivial topology in prototype compound $BaAl_4$, npj Quantum Mater. **6**, 28 (2021).

[4] F. Kneidinger, L. Salamakha, E. Bauer, I. Zeiringer, P. Rogl, C. Blaas-Schenner, D. Reith, and R. Podloucky, Superconductivity in noncentrosymmetric $BaAl_4$ derived structures, Phys. Rev. B **90**, 024504 (2014).

[5] A. Nakamura, T. Uejo, H. Harima, S. Araki, T. C. Kobayashi, M. Nakashima, Y. Amako, M. Hedo, T. Nakama, and Y. Ōnuki, Characteristic Fermi surfaces and charge density wave in $SrAl_4$ and related compounds with the $BaAl_4$-type tetragonal structure, J. Alloys Compd. **654**, 290 (2016).

[6] T. Shang, Y. Xu, D. J. Gawryluk, J. Z. Ma, T. Shiroka, M. Shi, and E. Pomjakushina, Anomalous Hall resistivity and possible topological Hall effect in the $EuAl_4$ antiferromagnet, Phys. Rev. B **103**, L020405 (2021).

[7] H. Zhang, X. Y. Zhu, Y. Xu, D. J. Gawryluk, W. Xie, S. L. Ju, M. Shi, T. Shiroka, Q. F. Zhan, E. Pomjakushina, and T. Shang,

Giant magnetoresistance and topological Hall effect in the $EuGa_4$ antiferromagnet, J. Phys.: Condens. Matter **34**, 034005 (2022).

[8] S. Araki, Y. Ikeda, T. C. Kobayashi, A. Nakamura, Y. Hiranaka, M. Hedo, T. Nakama, and Y. Ōnuki, Charge density wave transition in $EuAl_4$, J. Phys. Soc. Jpn. **83**, 015001 (2014).

[9] A. Nakamura, Y. Hiranaka, M. Hedo, T. Nakama, Y. Miura, H. Tsutsumi, A. Mori, K. Ishida, K. Mitamura, Y. Hirose, K. Sugiyama, F. Honda, T. Takeuchi, T. D. Matsuda, E. Yamamoto, Y. Haga, and Y. Ōnuki, Unique Fermi surface and emergence of charge density wave in $EuGa_4$ and $EuAl_4$, Jpn. Phys. Soc. Conf. Proc. **3**, 011012 (2014).

[10] A. Nakamura, T. Uejo, F. Honda, T. Takeuchi, H. Harima, E. Yamamoto, Y. Haga, K. Matsubayashi, Y. Uwatoko, M. Hedo, T. Nakama, and Y. Ōnuki, Transport and magnetic properties of $EuAl_4$ and $EuGa_4$, J. Phys. Soc. Jpn. **84**, 124711 (2015).

[11] S. Shimomura, H. Murao, S. Tsutsui, H. Nakao, A. Nakamura, M. Hedo, T. Nakama, and Y. Ōnuki, Lattice modulation and structural phase transition in the antiferromagnet $EuAl_4$, J. Phys. Soc. Jpn. **88**, 014602 (2019).

[12] M. Kobata, S. Fujimori, Y. Takeda, T. Okane, Y. Saitoh, K. Kobayashi, H. Yamagami, A. Nakamura, M. Hedo, T. Nakama, and Y. Ōnuki, Electronic structure of $EuAl_4$ studied by photoelectron spectroscopy, J. Phys. Soc. Jpn. **85**, 094703 (2016).

[13] J. M. Moya, S. Lei, E. M. Clements, K. Allen, S. Chi, S. Sun, Q. Li, Y. Y. Peng, A. Husain, M. Mitrano, M. J. Krogstad, R. Osborn, P. Abbamonte, A. B. Puthirath, J. W. Lynn, and E. Morosan, Incommensurate magnetic orders and possible field-induced skyrmions in the square-net centrosymmetric $EuGa_2Al_2$ system, arXiv:2110.11935.

[14] Y. Tokura and N. Kanazawa, Magnetic skyrmion materials, Chem. Rev. **121**, 2857 (2021), and references therein.

[15] A. Neubauer, C. Pfleiderer, B. Binz, A. Rosch, R. Ritz, P. G. Niklowitz, and P. Böni, Topological Hall effect in the *A* phase of MnSi, Phys. Rev. Lett. **102**, 186602 (2009).

[16] J. Gayles, F. Freimuth, T. Schena, G. Lani, P. Mavropoulos, R. A. Duine, S. Blügel, J. Sinova, and Y. Mokrousov, Dzyaloshinskii-Moriya Interaction and Hall Effects in the Skyrmion Phase of $Mn_{1-x}Fe_xGe$, Phys. Rev. Lett. **115**, 036602 (2015).

[17] N. Kanazawa, Y. Onose, T. Arima, D. Okuyama, K. Ohoyama, S. Wakimoto, K. Kakurai, S. Ishiwata, and Y. Tokura, Large Topological Hall Effect in a Short-Period Helimagnet MnGe, Phys. Rev. Lett. **106**, 156603 (2011).

[18] C. Franz, F. Freimuth, A. Bauer, R. Ritz, C. Schnarr, C. Duvinage, T. Adams, S. Blügel, A. Rosch, Y. Mokrousov, and C. Pfleiderer, Real-Space and Reciprocal-Space Berry Phases in the Hall Effect of $Mn_{1-x}Fe_xSi$, Phys. Rev. Lett. **112**, 186601 (2014).

[19] T. Kurumaji, T. Nakajima, M. Hirschberger, A. Kikkawa, Y. Yamasaki, H. Sagayama, H. Nakao, Y. Taguchi, T.-H. Arima, and Y. Tokura, Skyrmion lattice with a giant topological Hall effect in a frustrated triangular-lattice magnet, Science **365**, 914 (2019).

[20] M. Lee, W. Kang, Y. Onose, Y. Tokura, and N. P. Ong, Unusual Hall Effect Anomaly in MnSi under Pressure, Phys. Rev. Lett. **102**, 186601 (2009).

[21] Y. Li, N. Kanazawa, X. Z. Yu, A. Tsukazaki, M. Kawasaki, M. Ichikawa, X. F. Jin, F. Kagawa, and Y. Tokura, Robust Formation of Skyrmions and Topological Hall Effect Anomaly in Epitaxial Thin Films of MnSi, Phys. Rev. Lett. **110**, 117202 (2013).

[22] S. X. Huang and C. L. Chien, Extended Skyrmion Phase in Epitaxial FeGe(111) Thin Films, Phys. Rev. Lett. **108**, 267201 (2012).

[23] T. Schulz, R. Ritz, A. Bauer, M. Halder, M. Wagner, C. Franz, C. Pfleiderer, K. Everschor, M. Garst, and A. Rosch, Emergent electrodynamics of skyrmions in a chiral magnet, Nat. Phys. **8**, 301 (2012).

[24] Q. Qin, L. Liu, W. Lin, X. Shu, Q. Xie, Z. Lim, C. Li, S. He, G. M. Chow, and J. Chen, Emergence of topological Hall effect in a $SrRuO_3$ single layer, Adv. Mater. **31**, 1807008 (2019).

[25] J. Matsuno, N. Ogawa, K. Yasuda, F. Kagawa, W. Koshibae, N. Nagaosa, Y. Tokura, and M. Kawasaki, Interface-driven topological Hall effect in $SrRuO_3$-$SrIrO_3$ bilayer, Sci. Adv. **2**, e1600304 (2016).

[26] F. Jonietz, S. Mühlbauer, C. Pfleiderer, A. Neubauer, W. Münzer, A. Bauer, T. Adams, R. Georgii, P. Böni, R. A. Duine, K. Everschor, M. Garst, and A. Rosch, Spin transfer torques in MnSi at ultralow current densities, Science **330**, 1648 (2010).

[27] N. Nagaosa and Y. Tokura, Topological properties and dynamics of magnetic skyrmions, Nat. Nanotechnol. **8**, 899 (2013), and references therein.

[28] A. Fert, N. Reyren, and V. Cros, Magnetic skyrmions: Advances in physics and potential applications, Nat. Rev. Mater. **2**, 17031 (2017).

[29] M. Hirschberger, T. Nakajima, S. Gao, L. Peng, A. Kikkawa, T. Kurumaji, M. Kriener, Y. Yamasaki, H. Sagayama, H. Nakao, K. Ohishi, K. Kakurai, Y. Taguchi, X. Yu, T. Arima, and Y. Tokura, Skyrmion phase and competing magnetic orders on a breathing kagomé lattice, Nat. Commun. **10**, 5831 (2019).

[30] N. D. Khanh, T. Nakajima, X. Yu, S. Gao, K. Shibata, M. Hirschberger, Y. Yamasaki, H. Sagayama, H. Nakao, L. Peng, K. Nakajima, R. Takagi, T. Arima, Y. Tokura, and S. Seki, Nanometric square skyrmion lattice in a centrosymmetric tetragonal magnet, Nat. Nanotechnol. **15**, 444 (2020).

[31] K. Kaneko, T. Kawasaki, A. Nakamura, K. Munakata, A. Nakao, T. Hanashima, R. Kiyanagi, T. Ohhara, M. Hedo, T. Nakama, and Y. Ōnuki, Charge-density-wave order and multiple magnetic transitions in divalent europium compound $EuAl_4$, J. Phys. Soc. Jpn. **90**, 064704 (2021).

[32] T. Kawasaki, K. Kaneko, A. Nakamura, N. Aso, M. Hedo, T. Nakama, T. Ohhara, R. Kiyanagi, K. Oikawa, I. Tamura, A. Nakao, K. Munakata, T. Hanashima, and Y. Ōnuki, Magnetic structure of divalent europium compound $EuGa_4$ studied by single-crystal time-of-flight neutron diffraction, J. Phys. Soc. Jpn. **85**, 114711 (2016).

[33] A. Suter and B. M. Wojek, Musrfit: A free platform-independent framework for μSR data analysis, Phys. Procedia **30**, 69 (2012).

[34] A. Yaouanc and P. D. de Réotier, *Muon Spin Rotation, Relaxation, and Resonance: Applications to Condensed Matter* (Oxford University Press, Oxford, 2011)

[35] M. Fujita, K. M. Suzuki, S. Asano, H. Okabe, A. Koda, R. Kadono, and I. Watanabe, Magnetic behavior of T'-type Eu_2CuO_4 revealed by muon spin rotation and relaxation measurements, Phys. Rev. B **102**, 045116 (2020).

[36] L. M. Tran, M. Babij, L. Korosec, T. Shang, Z. Bukowski, and T. Shiroka, Magnetic phase diagram of Ca-substituted $EuFe_2As_2$, Phys. Rev. B **98**, 104412 (2018).

[37] Z. Guguchia, A. Shengelaya, A. Maisuradze, L. Howald, Z. Bukowski, M. Chikovani, H. Luetkens, S. Katrych, J. Karpinski, and H. Keller, Muon-spin rotation and magnetization studies of chemical and hydrostatic pressure effects in $EuFe_2(As_{1-x}P_x)_2$, J. Supercond. Nov. Magn. **26**, 285 (2013).
[38] J.-Z. Ma, S. M. Nie, C. J. Yi, J. Jandke, T. Shang, M. Y. Yao, M. Naamneh, L. Q. Yan, Y. Sun, A. Chikina, V. N. Strocov, M. Medarde, M. Song, Y.-M. Xiong, G. Xu, W. Wulfhekel, J. Mesot, M. Reticcioli, C. Franchini, C. Mudry *et al.*, Spin fluctuation induced Weyl semimetal state in the paramagnetic phase of $EuCd_2As_2$, Sci. Adv. **5**, eaaw4718 (2019).
[39] K. J. A. Franke, B. M. Huddart, T. J. Hicken, F. Xiao, S. J. Blundell, F. L. Pratt, M. Crisanti, J. A. T. Barker, S. J. Clark, A. Stefancic, M. C. Hatnean, G. Balakrishnan, and T. Lancaster, Magnetic phases of skyrmion-hosting $GaV_4S_{8-y}Se_y$ ($y = 0$, 2, 4, 8) probed with muon spectroscopy, Phys. Rev. B **98**, 054428 (2018).
[40] T. J. Hicken, M. N. Wilson, K. J. A. Franke, B. M. Huddart, Z. Hawkhead, M. Gomilsek, S. J. Clark, F. L. Pratt, A. Stefancic, A. E. Hall, M. Ciomaga Hatnean, G. Balakrishnan, and T. Lancaster, Megahertz dynamics in skyrmion systems probed with muon-spin relaxation, Phys. Rev. B **103**, 024428 (2021).
[41] V. Ukleev, K. Karube, P. M. Derlet, C. N. Wang, H. Luetkens, D. Morikawa, A. Kikkawa, L. Mangin-Thro, A. R. Wildes, Y. Yamasaki, Y. Yokoyama, L. Yu, C. Piamonteze, N. Jaouen, Y. Tokunaga, H. M. Rønnow, T. Arima, Y. Tokura, Y. Taguchi, and J. S. White, Frustration-driven magnetic fluctuations as the origin of the low-temperature skyrmion phase in $Co_7Zn_7Mn_6$, npj Quantum Mater. **6**, 40 (2021).
[42] S. Mulbauer, B. Binz, F. Jonietz, C. Pfleiderer, A. Rosch, A. Neubauer, R. Georgii, and P. Böni, Skyrmion lattice in a chiral magnet, Science **323**, 915 (2009).
[43] X. Z. Yu, N. Kanazawa, Y. Onose, K. Kimoto, W. Z. Zhang, S. Ishiwata, Y. Matsui, and Y. Tokura, Near room-temperature formation of a skyrmion crystal in thin-films of the helimagnet FeGe, Nat. Mater. **10**, 106 (2011).
[44] X. Z. Yu, Y. Onose, N. Kanazawa, J. H. Park, J. H. Han, Y. Matsui, N. Nagaosa, and Y. Tokura, Real-space observation of a two-dimensional skyrmion crystal, Nature (London) **465**, 901 (2010).
[45] S. Seki, X. Z. Yu, S. Ishiwata, and Y. Tokura, Observation of skyrmions in a multiferroic material, Science **336**, 198 (2012).
[46] I. Kézsmárki, S. Bordács, P. Milde, E. Neuber, L. M. Eng, J. S. White, H. M. Rønnow, C. D. Dewhurst, M. Mochizuki, K. Yanai, H. Nakamura, D. Ehlers, V. Tsurkan, and A. Loidl, Néel-type skyrmion lattice with confined orientation in the polar magnetic semiconductor GaV_4S_8, Nat. Mater. **14**, 1116 (2015).
[47] Y. Tokunaga, X. Z. Yu, J. S. White, H. M. Rønnow, D. Morikawa, Y. Taguchi, and Y. Tokura, A new class of chiral materials hosting magnetic skyrmions beyond room temperature, Nat. Commun. **6**, 7638 (2015).
[48] S. Seki, J.-H. Kim, D. S. Inosov, R. Georgii, B. Keimer, S. Ishiwata, and Y. Tokura, Formation and rotation of skyrmion crystal in the chiral-lattice insulator Cu_2OSeO_3, Phys. Rev. B **85**, 220406(R) (2012).
[49] H. Li, B. Ding, J. Chen, Z. Li, Z. Hou, E. Liu, H. Zhang, X. Xi, G. Wu, and W. Wang, Large topological Hall effect in a geometrically frustrated kagome magnet Fe_3Sn_2, Appl. Phys. Lett. **114**, 192408 (2019).
[50] Y. Xu, L. Das, J. Z. Ma, C. J. Yi, S. M. Nie, Y. G. Shi, A. Tiwari, S. S. Tsirkin, T. Neupert, M. Medarde, M. Shi, J. Chang, and T. Shang, Unconventional Transverse Transport Above and Below the Magnetic Transition Temperature in Weyl Semimetal $EuCd_2As_2$, Phys. Rev. Lett. **126**, 076602 (2021).
[51] C. D. Batista, S.-Z. Lin, S. Hayami, and Y. Kamiya, Frustration and chiral orderings in correlated electron systems, Rep. Prog. Phys. **79**, 084504 (2016).
[52] H. Niki, S. Nakamura, N. Higa, H. Kuroshima, T. Toji, M. Yogi, A. Nakamura, M. Hedo, T. Nakama, Y. Ōnuki, and H. Harima, Studies of ^{27}Al NMR in $EuAl_4$, J. Phys.: Conf. Ser. **592**, 012030 (2015).
[53] S. Heinze, K. von Bergmann, M. Menzel, J. Brede, A. Kubetzka, R. Wiesendanger, G. Bihlmayer, and S. Blügel, Spontaneous atomic-scale magnetic skyrmion lattice in two dimensions, Nat. Phys. **7**, 713 (2011).
[54] R. Ozawa, S. Hayami, and Y. Motome, Zero-Field Skyrmions with a High Topological Number in Itinerant Magnets, Phys. Rev. Lett. **118**, 147205 (2017).